Journal of Power Sources 195 (2010) 1302–1307

Contents lists available at ScienceDirect

Journal of Power Sources

journal homepage: www.elsevier.com/locate/jpowsour

Numerical determination of the effective thermal conductivity of fibrous materials. Application to proton exchange membrane fuel cell gas diffusion layers

D. Veyret, G. Tsotridis*

Institute for Energy, Joint Research Centre, European Commission, Postbus 2, 1755 ZG Petten, The Netherlands

ARTICLE INFO

Article history:
Received 26 June 2009
Received in revised form 2 September 2009
Accepted 10 September 2009
Available online 20 September 2009

Keywords:
Effective thermal conductivity
Fibrous material
Carbon fiber
PEFC
Numerical simulation

ABSTRACT

The knowledge of physical properties, such as the thermal conductivity, plays an important role in the management of the heat transfer in fibrous materials like PEFC gas diffusion layers. Measurement of thermal conductivity by experimental means is not easy (due to the anisotropy and the high porosity), therefore the availability of experimental data is rather limited. In this paper, the numerical determination of the effective thermal conductivity of fibrous materials is investigated using a three-dimensional approach. Two different fiber geometries were studied with randomly generated fiber structures with overlapping and non-overlapping fibers. The corresponding anisotropic thermal conductivities are computed through the solution of the energy transport equation. The results were validated through a comparison with existing experimental data and the influence of different parameters such as fiber orientation, fiber diameter and binding material were investigated.

1. Introduction

The solution of the purely diffusive steady state form of the heat transfer equation requires the knowledge of one physical property, namely the thermal conductivity. This property can be measured experimentally with different techniques [1], each depending on the type of material or the temperature range, and a high accuracy can be achieved in most of the cases. However, there are cases, such as fibrous materials, where the thermal conductivity is difficult to measure with high accuracy because of the stochastic nature of such materials and the strong influence of thermal contact between the fibers [2]. Many parameters can have a strong influence on its value such as porosity, fiber geometry (like diameter or shape), temperature range, fiber arrangement (isotropic or anisotropic), contact between fibers, ratio between matrix and fiber thermal conductivities, etc.

In order to overcome these experimental difficulties, numerous methods have been developed to predict the thermal conductivity such as analytical means, statistical methods, theoretical models, or numerical simulations [3–7]. However each of these methods has drawbacks, like idealized structures, empirical constants (adjustable parameters), or the need of heavy computing resources.

In this work, the effective thermal conductivity of fibrous materials has been evaluated by using a numerical model that minimizes the required computational resources. Due to the three-dimensional character of these simulations, several parameters can be taken into account and the full tensor of the thermal conductivity can be determined. The method was applied to gas diffusion layers of PEM fuel cells where the knowledge of the thermal conductivity is essential for the thermal management of such devices.

2. Numerical method

The computation of the effective thermal conductivity of fibrous materials requires the solution of the steady state, purely diffusive three-dimensional heat transfer equation. In the present approach, the convection and radiation transport, as well as thermal contact resistance and phase changes were not taken into account. The solution can be achieved by using several numerical schemes, such as finite differences or finite elements [3–5], by analytic methods [6], or by fractal method [7]. However, in the case of large three-dimensional geometries generated randomly or based on large data sets from digital imaging (like computer tomography), partial differential equation solvers are not efficient. The description of these complex geometries combined with the large difference in thermal conductivity of the matrix and fibers demand a very fine mesh, thereby requiring large amounts of memory and CPU time. Lately, lattice Boltzmann methods [8–11] have proved to overcome these limitations and can be very efficient

* Corresponding author. Tel.: +31 224 56 51 22; fax: +31 224 56 56 23.
E-mail addresses: damien.veyret@ec.europa.eu (D. Veyret), georgios.tsotridis@jrc.nl (G. Tsotridis).

0378-7753/$ – see front matter © 2009 Elsevier B.V. All rights reserved.
doi:10.1016/j.jpowsour.2009.09.028

Nomenclature

n_x, n_y, n_z	grid size
h	size of a voxel (μm)
v_f	fiber volume fraction
K	average value of the effective thermal conductivity ($W\,mK^{-1}$)
K_c	effective thermal conductivity of PCM44 with carbon fibers
K_{pcm}	effective thermal conductivity of PCM44

when working on large geometries. Weigmann and Zemitis [12] used a different approach, solving the energy equation by harmonic averaging and explicitly introducing discontinuities across the material interfaces as additional variables. These extra variables can be determined through the continuity of heat fluxes at the interfaces. Fast Fourier transform and BiCGStab methods are then used to solve the Schur-complement formulation for the new variables. The heat transfer equation in the purely diffusion form can be written as

$$\nabla \bullet (K\nabla T) = f \text{ in } \Omega \tag{1}$$

where T is the temperature, K is the local conductivity, f represents the heat sources or sinks and Ω is the domain considered.

Although the thermal conductivities of the materials constituting the fibrous media are considered in general as isotropic, the effective thermal conductivity of the fibrous material will be anisotropic due to the anisotropy of the geometry and it is fully described by the effective thermal conductivity tensor:

$$K^* = \begin{bmatrix} K^*_{11} & K^*_{12} & K^*_{13} \\ K^*_{21} & K^*_{22} & K^*_{23} \\ K^*_{31} & K^*_{32} & K^*_{33} \end{bmatrix}$$

The determination of the different components of this tensor can be performed using the homogenization theory. Three different singular periodic boundary value problems have to be solved:

$$\nabla \bullet (K(\vec{x})(\nabla T_n + \vec{e}_n)) = 0,\ x \in \Omega, \tag{2}$$

$$T_n(\vec{x} + id_1\vec{e}_1 + jd_2\vec{e}_2 + kd_3\vec{e}_3) = T_n(\vec{x})$$

with $n = (1, 2, 3)$, $\Omega = (0,d_1) \times (0,d_2) \times (0,d_3)$ and $\vec{e}_n$ is the unit vector in the respective direction. Having solved (2), the components of the averaged conductivity tensor can be computed by integrating the inner product of the evaluation direction i against the flux and vector in direction j:

$$K^*_{ij} = \frac{1}{d_1 d_2 d_3} \int_\Omega \langle \vec{e}_i, K(\vec{x})(\nabla T_j + \vec{e}_j)\rangle d\vec{x} \tag{3}$$

The difficulty in this approach consists in solving (2): the heat flux $K\nabla T_n$ is continuous only in directions perpendicular to $\vec{e}_n$ and has a discontinuity (or jump) in the direction $\vec{e}_n$ that is proportional to the difference in conductivities between the matrix and the fibers. These "jump" conditions can be also written as

$$[T_n]_{\vec{x}=\vec{x}^*} = 0$$

$$\left[K\frac{\partial T_n}{\partial x_i}\right]_{\vec{x}=\vec{x}^*} = -\delta_{in}[K]_{\vec{x}=\vec{x}^*}\ (i = 1, 2, 3)$$

where $[\,]_{\vec{x}=\vec{x}^*}$ is the jump across the interface at that position, ∂x_i is the directional derivative in the ith direction and δ_{in} is the Kronecker symbol.

Let us now consider a three-dimensional parallelepipedic domain of $n_1 \times n_2 \times n_3$ cubic voxels of size h^3. With t the discrete approximation of T, the harmonic averaging discretization of Eq. (1) on this grid is then

$$\begin{aligned}
&\frac{1}{h}\left(\left(\frac{1}{2K_{i+1,j,k}}+\frac{1}{2K_{i,j,k}}\right)^{-1}\frac{t_{i+1,j,k}-t_{i,j,k}}{h} - \left(\frac{1}{2K_{i,j,k}}+\frac{1}{2K_{i-1,j,k}}\right)^{-1}\right.\\
&\quad\times\frac{t_{i,j,k}-t_{i-1,j,k}}{h} + \left(\frac{1}{2K_{i,j+1,k}}+\frac{1}{2K_{i,j,k}}\right)^{-1}\frac{t_{i,j+1,k}-t_{i,j,k}}{h}\\
&\quad-\left(\frac{1}{2K_{i,j,k}}+\frac{1}{2K_{i,j-1,k}}\right)^{-1}\frac{t_{i,j,k}-t_{i,j-1,k}}{h}+\left(\frac{1}{2K_{i,j,k+1}}+\frac{1}{2K_{i,j,k}}\right)^{-1}\\
&\quad\left.\times\frac{t_{i,j,k+1}-t_{i,j,k}}{h} - \left(\frac{1}{2K_{i,j,k}}+\frac{1}{2K_{i,j,k-1}}\right)^{-1}\frac{t_{i,j,k}-t_{i,j,k-1}}{h}\right)\\
&= -\frac{K_{i,j,k}}{h}\left(\delta_{1l}\left(\frac{K_{i+1,j,k}-K_{i,j,k}}{K_{i+1,j,k}+K_{i,j,k}}+\frac{K_{i,j,k}-K_{i-1,j,k}}{K_{i,j,k}+K_{i-1,j,k}}\right)\right.\\
&\quad+\delta_{2l}\left(\frac{K_{i,j+1,k}-K_{i,j,k}}{K_{i,j+1,k}+K_{i,j,k}}+\frac{K_{i,j,k}-K_{i,j-1,k}}{K_{i,j,k}+K_{i,j-1,k}}\right)\\
&\quad\left.+\delta_{3l}\left(\frac{K_{i,j,k+1}-K_{i,j,k}}{K_{i,j,k+1}+K_{i,j,k}}+\frac{K_{i,j,k}-K_{i,j,k-1}}{K_{i,j,k}+K_{i,j,k-1}}\right)\right)
\end{aligned}$$

with $l = (1, 2, 3)$ representing the direction of the heat flux. Since the boundary conditions are supposed to be periodic, t_0 and t_{n_i+1} can be replaced, respectively by t_{n_i} and t_1.

For simplification, the derivation via jump conditions will be described in the following part only for i direction. The jump in the heat flux $\left[K(\partial T/\partial x_1)\right]_{i+(1/2),j,k}$ is discretized as

$$\begin{aligned}
&K_{i+1,j,k}\frac{T_{i+1,j,k}-T_{i+(1/2),jk}}{h/2} - K_{i,j,k}\frac{T_{i+(1/2)j,k}-T_{i,j,k}}{h/2}\\
&\quad= -\delta_{1l}(K_{i+1,j,k}-K_{i,j,k}) + O(h)
\end{aligned}$$

and a first order discretization of the condition of jump in the temperature gradient follows as

$$\left[\frac{\partial T}{\partial x_1}\right]_{i+(1/2),j,k} = -2\left(\frac{T_{i+1,j,k}-T_{i,j,k}}{h}+\delta_{1l}\right)\frac{K_{i+1,j,k}-K_{i,j,k}}{K_{i+1,j,k}+K_{i,j,k}} + O(h)$$

Using Taylor expansions in the presence of jumps, one finds

$$\begin{aligned}
&K_{i,j,k}\left(\frac{(T_{i+1,j,k}-(h/2)[\partial_{x_1}T]_{i+(1/2),j,k})-T_{i,j,k}}{h}\right.\\
&\quad-\frac{T_{i,j,k}-(T_{i-1,j,k}-(h/2)[\partial_{x_1}T]_{i-(1/2),j,k})}{h}\\
&\quad+\frac{(T_{i,j+1,k}-(h/2)[\partial_{x_2}T]_{i,j+(1/2),k})-T_{i,j,k}}{h}\\
&\quad-\frac{T_{i,j,k}-(T_{i,j-1,k}-(h/2)[\partial_{x_2}T]_{i,j-(1/2),k})}{h}\\
&\quad+\frac{(T_{i,j,k+1}-(h/2)[\partial_{x_3}T]_{i,j,k+(1/2)})-T_{i,j,k}}{h}\\
&\quad\left.-\frac{T_{i,j,k}-(T_{i,j,k-1}-(h/2)[\partial_{x_3}T]_{i,j,k-(1/2)})}{h}\right) = O(h)
\end{aligned}$$

After a division by $K_{i,j,k}$, the discretization of (2) with explicit jumps can be summarized as the discretization of the partial differential

equation:

$$\frac{t_{i+1,j,k}+t_{i-1,j,k}}{h^2}-\frac{\left\lfloor\partial_{x_1}t\right\rfloor_{i+(1/2),j,k}+\left\lfloor\partial_{x_1}t\right\rfloor_{i-(1/2),j,k}}{2h}$$
$$+\frac{t_{i,j+1,k}+t_{i,j-1,k}}{h^2}-\frac{\left\lfloor\partial_{x_2}t\right\rfloor_{i,j+(1/2),k}+\left\lfloor\partial_{x_2}t\right\rfloor_{i,j-(1/2),k}}{2h}$$
$$+\frac{t_{i,j,k+1}+t_{i,j,k-1}}{h^2}-\frac{\left\lfloor\partial_{x_3}t\right\rfloor_{i,j,k+(1/2)}+\left\lfloor\partial_{x_3}t\right\rfloor_{i,j,k-(1/2)}}{2h}$$
$$-\frac{6t_{i,j,k}}{h^2}=0 \quad (4)$$

and of the jump conditions (written here for the i direction for simplification):

$$2\frac{K_{i+1,j,k}-K_{i,j,k}}{K_{i+1,j,k}+K_{i,j,k}}\frac{t_{i+1,j,k}-t_{i,j,k}}{h}$$
$$+[\partial_{x_1}t]_{i+(1/2),j,k}=-2\delta_{1l}\frac{K_{i+1,j,k}-K_{i,j,k}}{K_{i+1,j,k}+K_{i,j,k}}$$

$$2\frac{K_{i,j,k}-K_{i-1,j,k}}{K_{i,j,k}+K_{i-1,j,k}}\frac{t_{i,j,k}-t_{i-1,j,k}}{h}$$
$$+[\partial_{x_1}t]_{i-(1/2),j,k}=-2\delta_{1l}\frac{K_{i,j,k}-K_{i-1,j,k}}{K_{i,j,k}+K_{i-1,j,k}}$$

The structure of (4) can also be rewritten in the following way:

$$\begin{bmatrix}A & \psi\\ D & I\end{bmatrix}\begin{bmatrix}T\\ J\end{bmatrix}=\begin{bmatrix}0\\ F\end{bmatrix}$$

where T is the vector of temperatures and J is the vector of nontrivial jumps. The Poisson problems associated to this system can then be solved efficiently using FFT, and J is solved iteratively using a BiCGStab solver.

Finally, the tensor of the effective thermal conductivity can be obtained by approximating (3):

$$K_{ij}\approx\frac{1}{d_1d_2d_3}\sum_{l=1}^{n_1}\sum_{m=1}^{n2}\sum_{p=1}^{n_3}K_{l,m,p}$$
$$\left(\frac{t_{l+1,m,p}-t_{l-1,m,p}}{2h}-\frac{\left\lfloor\partial_{x_1}t\right\rfloor_{l+(1/2),m,p}-\left\lfloor\partial_{x_1}t\right\rfloor_{l-(1/2),m,p}}{4}+\delta_{ij}\right)h^3$$

This method is implemented in an integrated simulation environment named GeoDict [13]. GeoDict was used in the current study to generate the structures and compute the effective thermal conductivity.

3. Results and discussion

3.1. Influence on numerical parameters on the results

Three-dimensional structures were generated by specifying geometric parameters such as fiber diameter and length, fiber volume fraction and the size of the grid ($n_x \times n_y \times n_z$). As expected, the generation of random structures cannot result in a single unique thermal conductivity tensor. The values fluctuate around an average, and the fluctuation is highly dependent on the size of the grid: a higher number of fibers will lead to a smaller fluctuation. This result is illustrated in Fig. 1 where more then 500 simulations were conducted for three different grid sizes ($n_x = n_y = n_z = 64$, 128 and 256). For each n, an average over the 500 simulations was performed and the dispersion of the conductivities around this average was plotted. For the smaller grid (i.e. $n = 64$) more than 30% of the structures show a deviation (larger than 9%) from the overall average value.

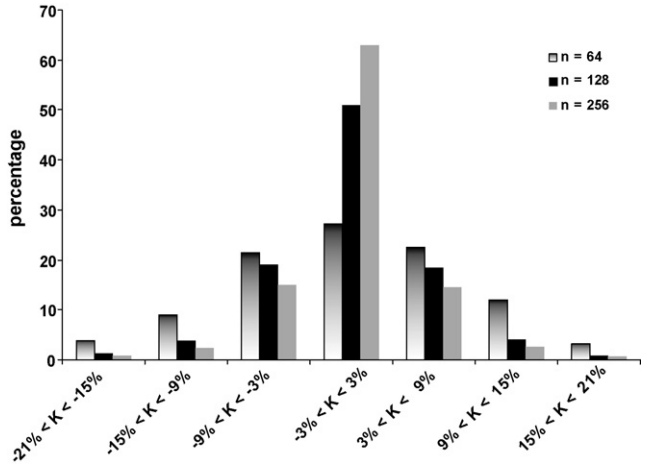

Fig. 1. Fluctuation of the effective thermal conductivity around the average value K for three different grid sizes ($n = 64$, 128, 256).

This number decreases to 10% and 6%, respectively for the larger grids ($n = 128$ and 256, respectively). The influence of the voxel size h has also been studied, and the value of 0.5 μm was chosen in the rest of the study: a bigger value has a negative effect on the precision of the results (the fibers are not described with enough precision) and a smaller value leads to too small structures.

Similarly, for a fixed grid size, a change in the fiber volume fraction will have an influence: the higher the fraction, the more fibers are included in the simulation and the smaller is the fluctuation (Fig. 2). However, the volume fraction size is intrinsic to the fibrous material and cannot be varied to ensure more precise numerical results.

In the following results, three-dimensional structures were generated using a grid size of $n = 256$ and each particular set of parameters was run 200 times in order to ensure high accuracy of results.

3.2. Comparisons and validation with experimental data

Frusteri et al. [14] studied experimentally the influence of carbon fibers on the thermal conductivity enhancement of an inorganic phase change material (PCM44). Carbon fibers of 6 μm diameter were added to the phase change material and the effective thermal conductivity was measured for different volume fraction loadings and different carbon fiber lengths for a range of aspect ratios (length/diameter) between 50 and 1000. In the current study,

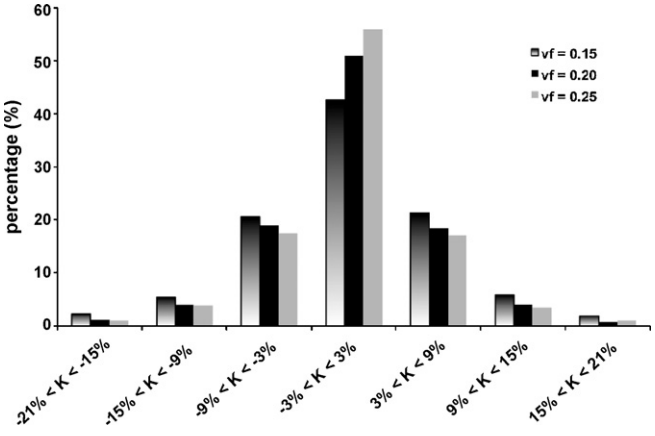

Fig. 2. Fluctuation of the effective thermal conductivity around the average value K for three different fiber volume fractions ($v_f = 0.15,\ 0.20,\ 0.25$; $n = 128$).

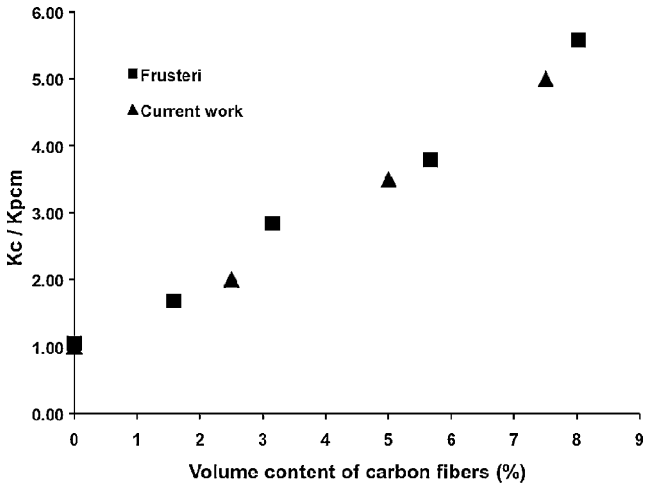

Fig. 3. Evolution of the effective thermal conductivity of PCM material with carbon fiber loading.

the influence of the fiber length was not investigated since it would have required a very large grid ($n > 500$) due to the large range of aspect ratios. The comparison for different volume fraction loadings between experimental results and the current numerical results is illustrated in Fig. 3. A good agreement can be observed for all volume fraction loadings for this case.

Khandelwal and Mench [15] measured the through-plane conductivities of Toray carbon papers without the addition of PTFE and compared them with the manufacturer specifications [16]. These results and the numerical predictions of the current work are summarized in Table 1 and they appear to be in good agreement. This comparison differs from the previous one by a higher volume fraction loading of carbon fibers, and the matrix composition (air vs. PCM).

3.3. Parametric study

3.3.1. Fiber radius, porosity and fiber arrangement

Fig. 4 shows the influence of the fiber diameter on the effective thermal conductivity at a constant porosity of 0.8, with an isotropic fiber arrangement. For a diameter up to 8 μm, the effective thermal conductivity remains constant and then decreases slowly for larger values. This effect can be explained that at a constant porosity, the increase in diameter implies fewer fibers, therefore less contact between them.

The influence of the porosity for an isotropic and anisotropic arrangement of fibers is illustrated in Fig. 5. As expected, a lower porosity leads to a higher value of the effective thermal conductivity for both cases (isotropic and anisotropic). The ratio between the thermal conductivity of the fiber over the thermal conductivity of the matrix is over 100: diminishing the porosity means more material with a higher conductivity.

In the anisotropic case, all the fibers lay parallel to the x–y plane (Fig. 6). The effect of the anisotropy (Fig. 5) is stronger for a high porosity, where the ratio between the in-plane and the through-plane conductivities is over 20, than for a low porosity where the same ratio is less than 5. The in-plane thermal conductivity benefits from the fibers length where there is little heat resistance compared to the through-plane conductivity where the matrix conductivity plays an important role.

Table 1
Through-plane thermal conductivity of Toray carbon paper (porosity: 0.78).

	Thermal conductivity ($W\,mK^{-1}$)
Manufacturer specification [16]	1.70
Khandelwal experiments [15]	1.80 ± 0.27
Current work (values averaged over 200 simulations)	1.86
	Tensor: $\begin{bmatrix} 9.790 & & \\ & 9.820 & \\ & & 1.860 \end{bmatrix}$

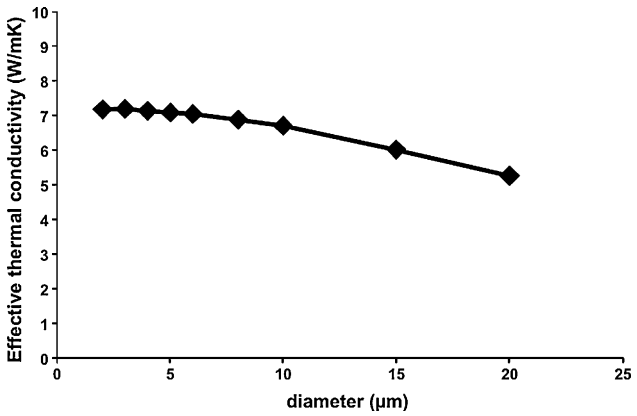

Fig. 4. Evolution of the effective thermal conductivity with carbon fiber diameter ($K_{fiber} = 120\,W\,mK^{-1}$; $K_{media} = 0.5\,W\,mK^{-1}$; porosity = 0.8—isotropic distribution of fibers).

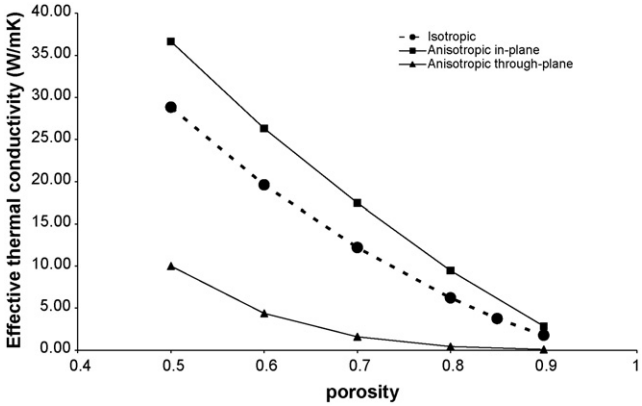

Fig. 5. Evolution of the effective thermal conductivity with the porosity for isotropic and anisotropic fibers arrangement.

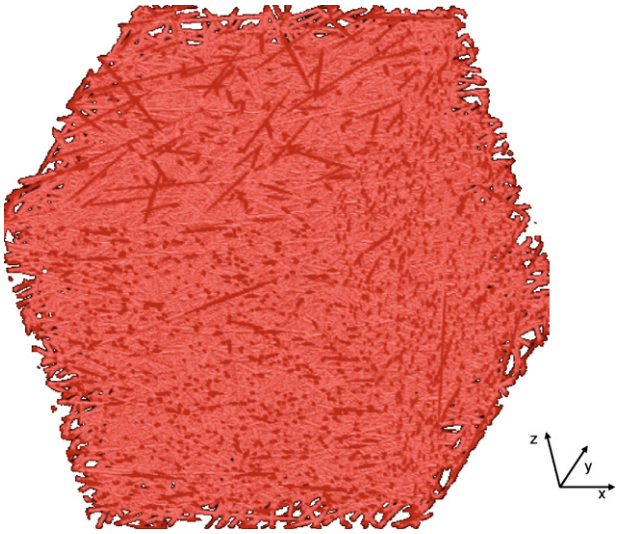

Fig. 6. Anisotropic arrangement of fibers.

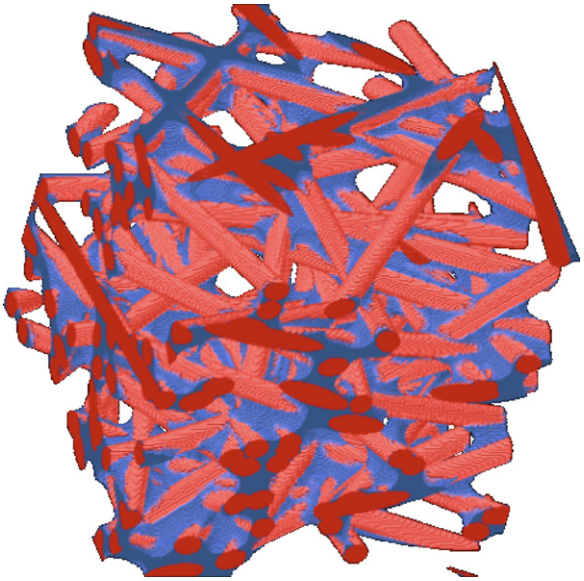

Fig. 7. 3D fibrous structure with 30 wt.% binder.

3.4. Binding effect

The carbon fibers constituting the gas diffusion layers of a PEM fuel cell are often pre-coated with polytetrafluoroethylene (PTFE), which has a knock-on effect of changing the material from hydrophilic to hydrophobic. PTFE (commonly known as Teflon) has two effects: it helps avoiding water flooding, and it acts as a binder to maintain the integrity of the material. Manufacturers commonly coat the carbon fibers with 10–30 wt.% of PTFE [17–20]. The presence of this coating has an effect on the effective thermal conductivity. Three-dimensional fiber structures were generated with different binder contents (Fig. 7) and their respective through-plane effective thermal conductivities were calculated and are presented in Fig. 8: the numerical results are close to the value of 1.7 W mK^{-1} reported by the manufacturer of the Toray carbon paper (TGP-H-060 without PTFE). The physical properties of the different materials considered in these simulations are presented in Table 2. The decrease of the effective thermal conductivity with increasing amount of Teflon can be explained as follows. The PTFE acts as an insulator around the carbon fibers and reduces the direct contact carbon to carbon. Since its thermal conductivity is almost 500 times smaller than that one of the carbon fibers, it overall reduces the effective thermal conductivity of the media. Similar behavior has also been noticed experimentally ([15,21]). This effect is well known in the heat exchanger field where alternative composite coatings (like nickel–phosphorous–PTFE) have successfully replaced ordinary PTFE coatings [22], due to their higher thermal conductivity.

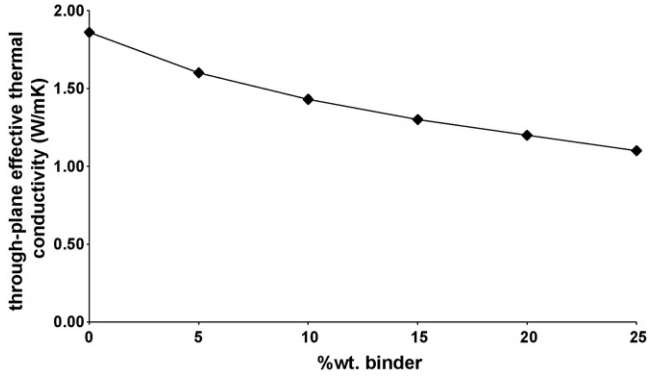

Fig. 8. Evolution of the through-plane effective thermal conductivity vs. binder loading (porosity: 0.8).

Table 2
Physical properties of carbon fibers, air and Teflon.

	Thermal conductivity (W mK^{-1})	Density (g cm^{-3})
Carbon fiber	130	1.8
Air	0.024	0.0013
PTFE	0.25	2.2

4. Conclusions

Three-dimensional structures have been randomly generated and the effective thermal conductivity for fibrous materials has been numerically determined under various configurations. Each set of parameters was run several times on a large grid, ensuring higher accuracy. Comparison between the results obtained from this work and experimental data obtained from literature and from manufacturers demonstrated a good agreement. The parametric study demonstrated that large fiber diameters reduce the effective thermal conductivity of the material, while an increase in the porosity leads to an almost linear decrease in the thermal conductivity. The anisotropy effect (in-plane vs. through-plane conductivity) is more pronounced for large porosity, where the contacts within fiber (which lay horizontally) are reduced. Finally, the binding of the fibers with a material of low conductivity (like PTFE) has a decreasing effect on the effective thermal conductivity.

Acknowledgements

This work has been carried out within the multi-year programme of the European Commission's Joint Research Centre, under the auspices of the FCPOINT activities. The authors would like to thank Marc Steen for critical reading of the manuscript. This document does not represent the point of view of the European Commission. Any interpretations or opinions contained in this document are solely those of the authors.

References

[1] K. Maglic, A. Cezairliyan, V.E. Peletsky, Springer Ed (1992) ISBN 0306438542.
[2] P. Furmanski, J. Thermoplast. Compos. Mater. 4 (1991) 349–362.
[3] T. Sakiyama, Y. Matsushita, Y. Shiinoki, T. Yano, J. Food Eng. 11 (1990) 317–331.
[4] D. Veyret, S. Cioulachtjian, L. Tadrist, J. Pantaloni, J. Heat Transfer 115 (1993) 866–871.
[5] K.H. Chua, T.F. Fwa, A. Shein, Comp. Geol. 14 (1992) 43–55.
[6] E. Sadeghi, M. Bahrami, N. Djilali, J. Power Sources 179 (2008) 200–208.
[7] Y.S. HI, J. Xiao, S. Quan, M. Pan, R. Yuan, J. Power Sources 185 (2008) 241–247.
[8] M. Wang, J. He, J. Yu, N. Pan, Int. J. Therm. Sci. 46 (2007) 848–855.
[9] M. Wang, Q. Kang, N. Pan, Appl. Therm. Eng. 29 (2009) 418–421.
[10] M. Wang, J.K. Wang, N. Pan, S.Y. Chen, Phys. Rev. E 75 (2007) 036702.
[11] M. Wang, J.K. Wang, N. Pan, S.Y. Chen, J.H. He, J. Phys. D: Appl. Phys. 40 (2007) 260–265.
[12] A. Weigmann, A. Zemitis, Fraunhofer ITWM Technical report Nr 94 (2006).
[13] GeoDict, www.geodict.com.
[14] F. Frusteri, V. Leonardi, S. Vasta, G. Restuccia, Appl. Therm. Eng. 25 (2005) 1623–1633.
[15] M. Khandelwal, M.M. Mench, J. Power Sources 161 (2006) 1106–1115.
[16] Toray carbon paper—manufacturer data sheet, www.torayca.com/index2.html.
[17] V.A. Paganin, E.A. Ticianelli, E.R. Gonzalez, J. Appl. Electrochem. 26 (1996) 297–304.

[18] L. Giorgi, E. Antolini, A. Pozio, E. Passalacqua, Electrochim. Acta 43 (1998) 3675–3680.
[19] F. Lufrano, E. Passalacqua, G. Squadrito, A. Patti, L. Giorgi, J. Appl. Electrochem. 29 (1999) 445–448.
[20] E. Antolini, R.R. Passos, E.A. Ticianelli, J. Appl. Electrochem. 32 (2002) 383–388.
[21] J. Ramousse, S. Didierjean, O. Lottin, D. Maillet, Int. J. Therm. Sci. 47 (2008) 1–6.
[22] Q. Zhao, Y. Liu, H. Müller-Steinhagen, G. Liu, Surf. Coat. Technol. 155 (2002) 279–284.